

# Break-up effect of the weakly bound ${}^6\text{Li}$ ions scattered by ${}^{208}\text{Pb}$ target

Sh. Hamada

*Faculty of Science, Tanta University, Tanta, Egypt.*

N. Burtebayev

*Institute of Nuclear Physics, Almaty, Kazakhstan,  
Al-Farabi Kazakh National University, Almaty, Kazakhstan.*

Awad A. Ibraheem

*Physics Department, King Khalid University, Abha, Saudi Arabia,  
Physics Department, Al-Azhar University, Assiut Branch, Assiut 71524, Egypt.*

Received 23 October 2021; accepted 11 November 2021

Using different potentials based on phenomenological, semi microscopic, and microscopic models, we investigated the reaction dynamics induced by the weakly bound  ${}^6\text{Li}$  ions on a heavy mass target  ${}^{208}\text{Pb}$  at sixteen energy sets ranging from 25 MeV to 210 MeV. The  ${}^6\text{Li}$  cluster nature and its dissociation into a core ( $\alpha$ -particle) and a valence particle (deuteron) orbiting this core was taken into consideration using the cluster folding model (CFM). The new version of Sao Paulo potential (SPP2) is also used to investigate  ${}^6\text{Li}+{}^{208}\text{Pb}$  data. In order to reproduce the experimental data, the strength of real part of potential created using SPP and CFM should be reduced by  $\sim 49\%$  and  $62\%$ , respectively. The data could be well reproduced using non-renormalized real cluster folding potential, if an additional dynamical polarization potential (DPP) of repulsive real surface form is introduced. The observed reduction in the strength of the real double folded and cluster folding potentials is due to the break-up effect of  ${}^6\text{Li}$ .

**Keywords:** Elastic scattering; Sao Paulo potential; phenomenological potential; Cluster folding; dynamical polarization potential.

DOI: <https://doi.org/10.31349/RevMexFis.68.031201>

## 1. Introduction

The break-up effect observed in many nuclear systems induced by loosely bound nuclei  ${}^6\text{Li}$ ,  ${}^7\text{Li}$  and  ${}^9\text{Be}$ , and by exotic nuclei  ${}^6\text{He}$  (2n-halo nucleus),  ${}^8\text{He}$  (neutron skin nucleus),  ${}^{11}\text{Be}$ , and  ${}^{12}\text{Be}$  scattered by different targets attracted a plenary attention for decades. One of the most interesting nuclear systems where break-up effect could be observed is  ${}^6\text{Li}+{}^{208}\text{Pb}$  system. Extensive experimental [1–10] and theoretical [11–25] studies were and still are being devoted to investigate  ${}^6\text{Li}+{}^{208}\text{Pb}$  nuclear system at various energies both near and above the Coulomb barrier energy  $E_C$ . Chun-Lei *et al.* [1] measured the elastic scattering angular distributions for  ${}^6\text{Li}+{}^{208}\text{Pb}$  system at energies 25, 27, 29, 31, 33, 35, 37, 41, 43, and 46 MeV. These data were analyzed from the phenomenological point of view using optical model (OM). The extracted real and imaginary potential depths showed pronounced energy dependence. The behavior of the extracted potential is found to be quite different in comparison with other systems such as  ${}^{19}\text{F}$ ,  ${}^{16}\text{O}+{}^{208}\text{Pb}$ . This anomaly is a signature of break-up effect resulting from weak binding nature of  ${}^6\text{Li}$  and hence has obvious effect on optical potentials. Keeley *et al.*, [2] measured the  ${}^6\text{Li}+{}^{208}\text{Pb}$  elastic scattering angular distributions in the energy range  $E_{lab} = 25\text{--}39$  MeV. The measured differential cross sections were analyzed using a real part derived based on double folding (DF) model in addition to an imaginary part of the conventional Woods-Saxon (WS) shape. The main finding of this study was the necessity to reduce the strength of the real folded potential

by 43 % in order to reasonably reproduce the data, which is consistent with a repulsive polarization potential arising from the effects of break-up coupling to the continuum. In Ref. [3], the  ${}^6\text{Li}+{}^{208}\text{Pb}$  angular distributions were measured in the energy range 23–48 MeV in order to find a unique description of the sequential  $d + \alpha$  break-up of  ${}^6\text{Li}$  in the field of heavy target nuclei. The measured data were analyzed using central nuclear potential of three parts: real and imaginary volume terms in addition to an imaginary surface term each of WS shape. In Ref. [4], the authors tried to provide optical model parameters for the scattering of  ${}^6\text{Li}$  at energy 73.7 MeV on different medium and high mass targets:  ${}^{58}\text{Ni}$ ,  ${}^{90}\text{Zr}$ ,  ${}^{124}\text{Sn}$ , and  ${}^{208}\text{Pb}$ . The dependence of the potential depths on the Z and A of the considered targets and on the bombarding energy was investigated. Fulmer *et al.* [5] measured the angular distributions for 88-MeV  ${}^6\text{Li}$  ions elastically scattered from eleven targets ranging in mass from  ${}^{24}\text{Mg}$  to  ${}^{208}\text{Pb}$ . The elastic data were analyzed using the optical model, with potentials of both WS and DF forms. The analysis confirmed that the potentials for  ${}^6\text{Li}$  obtained from the DF model with the M3Y interaction need renormalizing by about 0.6. In Ref. [6], the differential cross section angular distributions for 99-MeV  ${}^6\text{Li}$  ions elastically scattered from  ${}^{12}\text{C}$ ,  ${}^{28}\text{Si}$ ,  ${}^{40}\text{Ca}$ ,  ${}^{58}\text{Ni}$ ,  ${}^{90}\text{Zr}$ , and  ${}^{208}\text{Pb}$  targets were measured. By increasing the target mass, the angular distributions showed progressively less structure which is characteristic of strongly absorbed particles. The analyzed data using OM exhibited both discrete and continuous ambiguities. The data

also were analyzed using single folding  ${}^6\text{Li}$  potential based on  $d + \alpha$  cluster model for  ${}^6\text{Li}$ , a satisfactory description of the data was obtained only after renormalization of the real potential by a factor of 0.5. J. Cook *et al.* [7] measured the elastic scattering angular distributions for 156- MeV  ${}^6\text{Li}$  ions from  ${}^{12}\text{C}$ ,  ${}^{40}\text{Ca}$ ,  ${}^{90}\text{Zr}$ , and  ${}^{208}\text{Pb}$ . The data were analyzed using various potential forms established by using WS, WS squared and density independent folded potentials. The data analysis emphasized the necessity to reduce the real folded potential strength by about 21-44 % according to the target mass. The experimental measurements were continued to test this behavior for nuclear reactions induced by  ${}^6\text{Li}$  at higher energies. In Ref. [8], the differential cross sections for the elastic scattering of 210- MeV  ${}^6\text{Li}$  ions on different target nuclei “ ${}^{12}\text{C}$ ,  ${}^{28}\text{Si}$ ,  ${}^{40}\text{Ca}$ ,  ${}^{58}\text{Ni}$ ,  ${}^{90}\text{Zr}$ , and  ${}^{208}\text{Pb}$ ” were measured. Most of the measured data were extended sufficiently into the rainbow region to enable the extraction of unique  ${}^6\text{Li}$  potentials. For the  ${}^{208}\text{Pb}$  target, Coulomb scattering dominates with only a slight evidence of nuclear diffraction at the largest angles. The data were analyzed in terms of a six-parameter phenomenological OM potential with WS form factors. The obtained unique potentials showed a weak target-mass dependence, which allowed the prediction of  ${}^{208}\text{Pb}$  potential parameters.

Furthermore, it is worth to underline that recent experimental evidences for Li-isotopes and a few of similar nuclei lying in the nuclide-chart close to  ${}^6\text{Li}$  seem to show the behavior looks similar [26,27] or at most with small differences, to the above described one, *i.e.* with enhancement of nuclear effects at large angles, mainly at energy around the Coulomb barrier. A partial response to the interesting question which could arise, if and how structure effects, such as in particular cluster configuration, could play a role in this respect for close nuclides in this region, can be found in [28].

In addition to these extensive measurements, different theoretical studies [11–16] were also devoted to investigate  ${}^6\text{Li}$ +nucleus potential and the break-up effect of  ${}^6\text{Li}$  into  $d + \alpha$  on the elastic scattering data. Yongli Xu *et al.* [11] established a systematic global phenomenological OM potential for  ${}^6\text{Li}$  projectile by studying the experimental data of elastic scattering angular distributions and reaction cross sections from  ${}^{24}\text{Mg}$  to  ${}^{209}\text{Bi}$  below 250 MeV. Based on the obtained  ${}^6\text{Li}$  global phenomenological OM, the theoretical calculations using the global OM potential was consistent with a large body of elastic-scattering data. In Ref. [14], the angular distributions for  ${}^{6,7}\text{Li}$  elastically scattered from  ${}^{12}\text{C}$ ,  ${}^{28}\text{Si}$ ,  ${}^{40}\text{Ca}$ ,  ${}^{58}\text{Ni}$ ,  ${}^{90}\text{Zr}$  and  ${}^{208}\text{Pb}$  targets at 12.5 – 53 MeV/u were analyzed utilizing a real part of potential constructed using Jeukenne, Lejeune and Mahaux (*JLM*) method and a Gaussian shape of the effective  $NN$  nucleon–nucleon interaction. An energy dependent reducing renormalization coefficient was required for the real component of the *JLM* optical potential in order to obtain successful predictions of the observed cross sections even when the projectile density-dependence was considered.

Several microscopic studies investigated the break-up effect in  ${}^6\text{Li}$  projectile [17–25], Watanabe *et al.* [17] investigated break-up dynamics in  ${}^6\text{Li}$  elastic scattering on  ${}^{208}\text{Pb}$  at  $E = 39$  MeV using both three-body channel ( ${}^6\text{Li} + {}^{208}\text{Pb} \rightarrow d + \alpha + {}^{208}\text{Pb}$ ) and four-body channel ( ${}^6\text{Li} + {}^{208}\text{Pb} \rightarrow n + p + \alpha + {}^{208}\text{Pb}$ ). Both channels are precisely treated with the four-body version of the continuum-discretized coupled-channels method (four-body CDCC). The main finding of this study is that  ${}^6\text{Li}$  break-up is mainly induced by a three-body channel. In Ref. [24], elastic scattering of  ${}^6\text{Li}$  from various targets:  ${}^{12}\text{C}$ ,  ${}^{28}\text{Si}$ ,  ${}^{58}\text{Ni}$ ,  ${}^{120}\text{Sn}$  and  ${}^{208}\text{Pb}$  nuclei at various incident energies up to 100 MeV per nucleon was investigated by the CDCC method based on a double folding model of the  ${}^6\text{Li}$  nucleus interaction with a realistic energy and density dependent  $NN$  interaction, called DDM3Y. The  ${}^6\text{Li}$  projectile break-up effect is found to diminish with increasing incident energies.

The current study aims to investigate the available  ${}^6\text{Li}+{}^{208}\text{Pb}$  elastic scattering angular distributions in a wide energy range and at energies both near and above the Coulomb barrier energy  $E_C$  using different potentials, and to observe the break-up effect of  ${}^6\text{Li}$  into  $d + \alpha$  on the  ${}^6\text{Li}+{}^{208}\text{Pb}$  elastic scattering data. This work supplements our previous studies for different nuclear systems induced by the weakly bound  ${}^6\text{Li}$  ions [29–32]. The paper is organized as follows. Section 2 demonstrates the different potentials used in theoretical calculations. Section 3 is devoted to data analysis, results and discussion. Summary is given in Sec. 4.

## 2. Theoretical methods

The elastic scattering angular distributions for  ${}^6\text{Li} + {}^{208}\text{Pb}$  nuclear system in the energy range 25 – 210 MeV are subjected to detailed theoretical analysis using different potentials created based on phenomenological, semi-microscopic, and microscopic models. The current study aims to obtain the global potential that fairly reproduce the experimental data in this wide range of energies and to observe how the interaction mechanism differ as we go from near barrier energy to the region of relatively higher energies. In addition, the  ${}^6\text{Li}$  break-up effect was observed on the elastic scattering data as well as the various incorporated models.

### 2.1. Phenomenological OM potential

The data on elastic scattering were firstly analyzed from the phenomenological point of view within the framework of the standard optical model of the nucleus, where the influence of inelastic channels is taken into account by introducing a phenomenological imaginary absorptive part in the interaction potential between the two colliding nuclei. In this model the elastic scattering is described by a complex interaction potential with a radial dependence in the form of WS. For both the real and imaginary parts of the potential, the WS shape is taken in addition to the Coulomb potential of a uniformly charged sphere. So, the utilized interaction potential can be

written as:

$$U(r) = V_C - V_0 \left[ 1 + \exp\left(\frac{r - R_V}{a_V}\right) \right]^{-1} - iW_0 \left[ 1 + \exp\left(\frac{r - R_W}{a_W}\right) \right]^{-1}, \quad (1)$$

with radius  $R_i = r_i(A_T^{1/3})$ ,  $i = V, W, C$

Parameters of optical potential (OP) were selected to achieve the best agreement between theoretical and experimental angular distributions. The  $\chi^2$  value, which is the measure for the deviation of theoretical calculations from experimental measurements, is defined by:

$$\chi^2 = \frac{1}{N} \sum_{i=1}^N \left( \frac{\sigma(\theta_i)^{\text{cal}} - \sigma(\theta_i)^{\text{exp}}}{\Delta\sigma(\theta_i)} \right)^2, \quad (2)$$

where  $N$  is the number of data points. The quantities  $\sigma(\theta_i)^{\text{cal}}$  and  $\sigma(\theta_i)^{\text{exp}}$  are the calculated and experimental differential cross sections, while the quantity  $\Delta\sigma(\theta_i)$  is the relative uncertainty in experimental data. The theoretical calculations as well as searching for the optimal potential parameters were performed using FRESCO and SFRESCO search code [33].

## 2.2. Sao Paulo potential

According to the different parameter ambiguities both discrete and continuous associated with the OM calculations, and the fact that phenomenological representations do not include a description of the projectile or target's structure, the real part of potential was constructed using the microscopic double folding (DF) procedure extracted from the Sao Paulo potential (SPP) via the double convolution integral as described in Refs. [34–36].

$$V_F(R) = \iint \rho_P(r_P) \rho_T(r_T) V_0 \delta\left(\left|\vec{s}\right|\right) d^3r_P d^3r_T, \quad (3)$$

$$\vec{s} = \vec{R} - \vec{r}_P + \vec{r}_T,$$

where  $\rho_P(r_P)$  and  $\rho_T(r_T)$ , are the nuclear matter density distributions of  ${}^6\text{Li}$  and  ${}^{208}\text{Pb}$  nuclei, respectively, with  $V_0 = -456$  MeV.

In this model, the following two equations link the real part of the local-equivalent interaction to the DF potential  $V_F(R)$  as

$$V_N(R, E) = V_F(R) e^{-\frac{4V^2}{c^2}} \quad (4)$$

$$V^2(R, E) = \frac{2}{\mu} [E - V_C(R) - V_N(R, E)], \quad (5)$$

where  $V$  is the local relative velocity between the two nuclei and  $C$  is the speed of light. The new version of the Sao Paulo potential (SPP2) was calculated using the REGINA code [37] with nuclear densities obtained from the Dirac-Hartree-Bogoliubov model [38].

## 2.3. Cluster folding potential

The  ${}^6\text{Li} + {}^{208}\text{Pb}$  elastic scattering data are analyzed from microscopic point of view using the cluster folding model (CFM). The importance of various break-up mechanisms in nuclear systems induced by  ${}^6\text{Li}$  is of special interest due to its very low binding energy and the dissociation into  $\alpha$  (*core*) +  $d$  (*valence*). Based on the cluster nature of  ${}^6\text{Li}$ , we describe the  ${}^6\text{Li} + {}^{208}\text{Pb}$  elastic scattering angular distributions using CFM where, both the real and imaginary parts of potential are created based on cluster folding. The real and imaginary cluster folding parts of  ${}^6\text{Li} + {}^{208}\text{Pb}$  potential can be defined based on  $\alpha + {}^{208}\text{Pb}$  and  $d + {}^{208}\text{Pb}$  potentials as:

$$V^{CF}(R) = \int \left( V_{\alpha-{}^{208}\text{Pb}} \left[ \mathbf{R} - \frac{1}{3}\mathbf{r} \right] + V_{d-{}^{208}\text{Pb}} \left[ \mathbf{R} + \frac{2}{3}\mathbf{r} \right] \right) |\chi_{\alpha d}(\mathbf{r})|^2 d\mathbf{r}, \quad (6)$$

$$W^{CF}(R) = \int \left( W_{\alpha-{}^{208}\text{Pb}} \left[ \mathbf{R} - \frac{1}{3}\mathbf{r} \right] + W_{d-{}^{208}\text{Pb}} \left[ \mathbf{R} + \frac{2}{3}\mathbf{r} \right] \right) |\chi_{\alpha d}(\mathbf{r})|^2 d\mathbf{r}, \quad (7)$$

where  $(V_{\alpha-{}^{208}\text{Pb}}, V_{d-{}^{208}\text{Pb}})$  and  $(W_{\alpha-{}^{208}\text{Pb}}, W_{d-{}^{208}\text{Pb}})$  are the real and imaginary parts of potentials for  $\alpha + {}^{208}\text{Pb}$  and  $d + {}^{208}\text{Pb}$  channels which fairly reproduce the experimental data at the appropriate energies  $E_d \approx 1/3 E_{Li}$  and  $E_\alpha \approx 2/3 E_{Li}$  taken from Refs. [39, 40].  $\chi_{\alpha d}(\mathbf{r})$  is the intercluster wave function for the relative motion of  $\alpha$  and  $d$  in the ground state of  ${}^6\text{Li}$ , and  $\mathbf{r}$  is the relative coordinate between the centres of mass of  $\alpha$  and  $d$ . The  $\alpha$ - $d$  bound state form factor represents a  $2S$  state in a real WS potential with  $V_0 = 79.0$  MeV,  $R = 1.83$  fm,  $a = 0.7$  fm [6] plus Coulomb potential. The main parameters required to prepare the cluster folding potential for  ${}^6\text{Li} + {}^{208}\text{Pb}$  are the optimal potentials for  $d + {}^{208}\text{Pb}$  and  $\alpha + {}^{208}\text{Pb}$  at appropriate energies. The highest energy under consideration is 210 MeV, so the required potentials are  $V_{d-{}^{208}\text{Pb}}$  at  $E_{lab} = 1/3 \times 210 = 70$  MeV and  $V_{\alpha-{}^{208}\text{Pb}}$  at  $E_{lab} = 2/3 \times 210 = 120$  MeV. By searching through the previous experimental studies for  $d + {}^{208}\text{Pb}$  and  $\alpha + {}^{208}\text{Pb}$  nuclear systems, the most suitable potentials which could be used to generate the cluster folding potential for  ${}^6\text{Li} + {}^{208}\text{Pb}$  are:  $d + {}^{208}\text{Pb}$  at  $E_{lab} = 80$  MeV [39] and  $\alpha + {}^{208}\text{Pb}$  at  $E_{lab} = 139$  MeV [40]. These potentials are used to generate the real and imaginary CF potentials expressed in Eqs. (6) and (7) as shown in Fig. 1.

## 3. Results and discussion

### 3.1. ${}^6\text{Li} + {}^{208}\text{Pb}$ data analysis using phenomenological OM potential

Within the framework of OM, the available angular distributions for  ${}^6\text{Li}$  elastically scattered from  ${}^{208}\text{Pb}$  in the energy

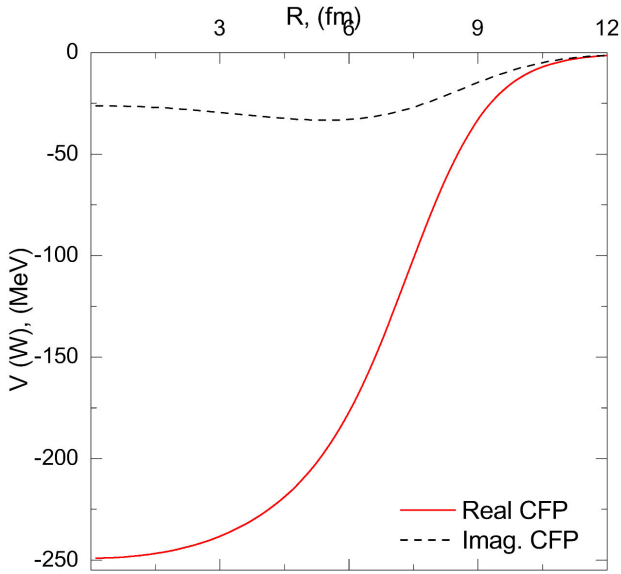


FIGURE 1. Real and imaginary cluster folding potentials used in the current study.

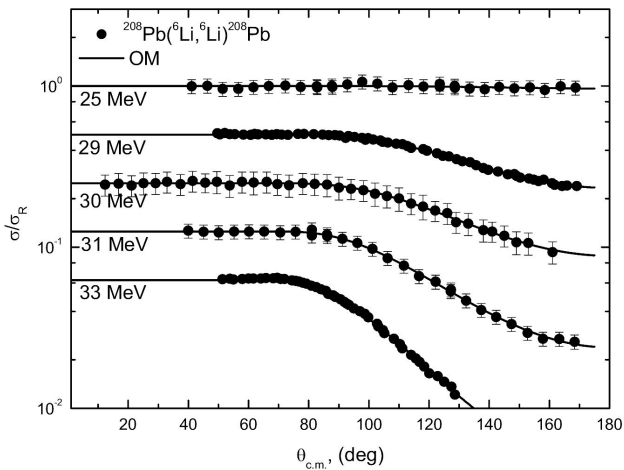


FIGURE 2. Comparison between  $^{208}\text{Pb}(^6\text{Li}, ^6\text{Li})^{208}\text{Pb}$  elastic scattering angular distributions (solid circles) and OM (solid curves) fits at  $E_{lab} = 25, 29, 30, 31,$  and  $33$  MeV. The data are displaced by 0.5 for the sake of clarity.

range 25 - 210 MeV [1–8] have been reanalyzed. The potential parameters considered by C. Fulmer *et al.* [5] for both the real and imaginary parts of potential are taken as starting parameters. The utilized central potential consists of Coulomb part as well as nuclear part of real and imaginary volume terms each of WS shape. In accordance with previous studies concerning nuclear processes induced by  $^6\text{Li}$ -projectile, the influence of spin orbit potential ( $V_{SO}$ ) for  $^6\text{Li}$  is little and its effect can be excluded. Data are fitted using four varying parameters, namely, depth and diffuseness for the real ( $V_0$  and  $a_V$ ) and imaginary ( $W_0$  and  $a_W$ ) parts of the potential. Where, the radius parameters for the real ( $r_V$ ) and imaginary ( $r_W$ ) parts was fixed at 1.3 fm and 1.7 fm, respectively. The agreement between the experimental  $^6\text{Li} + ^{208}\text{Pb}$  elastic scattering angular distributions and the theoretical cal-

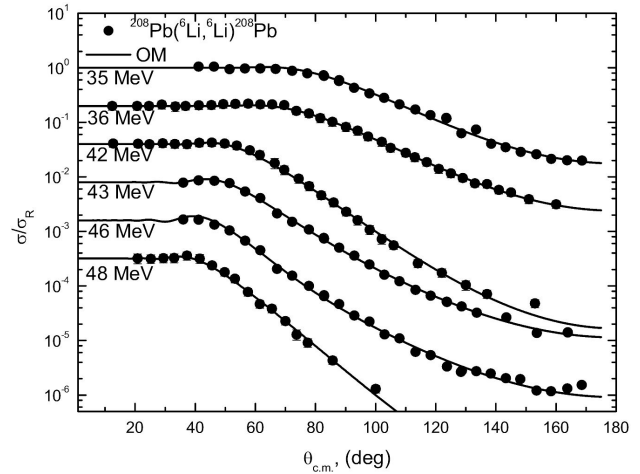


FIGURE 3. Same as Fig. 2 but at  $E_{lab} = 35, 36, 42, 43, 46$  and  $48$  MeV. The data are displaced by 0.2 for the sake of clarity.

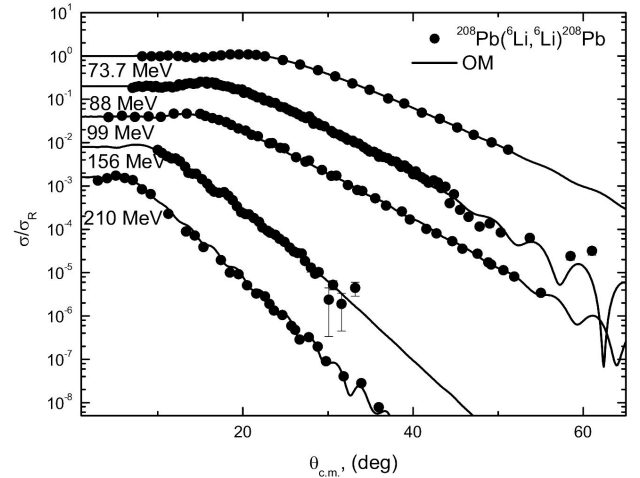


FIGURE 4. Same as Fig. 2 but at  $E_{lab} = 73.7, 88, 99, 156$  and  $210$  MeV. The data are displaced by 0.2 for the sake of clarity.

culations using OM is fairly good at the different considered energies as shown in Figs. 2-4. The extracted optimal OM parameters are listed in Table I, real ( $J_V$ ) and imaginary ( $J_W$ ) volume integrals as well as total reaction cross section ( $\sigma_R$ ) values are also presented.

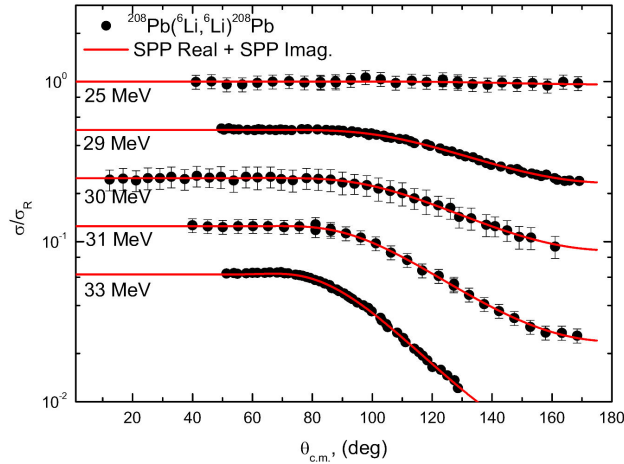
As shown from Figs. 2-4,  $^6\text{Li} + ^{208}\text{Pb}$  data show unmistakable Coulomb rainbow phenomenon which results in the so called Fresnel peak. It is pronounced that the position of this peak is shifted toward smaller angles with increasing the bombarding energy. At lowest energy 25 MeV which is very close to  $E_C$ , this peak is not presented and it starts to be clearly appear at  $E > 33$  MeV which is slightly above  $E_C$ .

### 3.2. $^6\text{Li} + ^{208}\text{Pb}$ data analysis using Sao Paulo potential

The  $^6\text{Li} + ^{208}\text{Pb}$  elastic scattering angular distributions are then analyzed semi-microscopically using SPP. Two approaches were used: in the first approach, the real part of the potential was derived using SPP and the imaginary part

TABLE I. Global potential parameters extracted from the OM analysis for the  ${}^6\text{Li} + {}^{208}\text{Pb}$  nuclear system with fixed  $r_V = 1.3$  fm and  $r_W = 1.7$  fm. Real and imaginary volume integrals as well as reaction cross-sections are also listed.

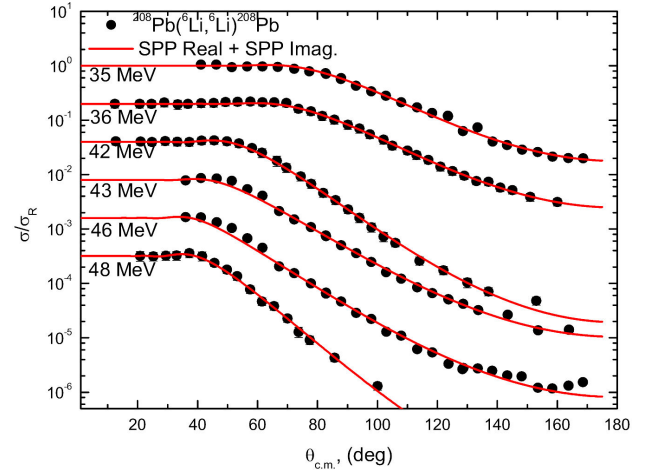
$E$ (MeV)	$V_0$ (MeV)	$a_V$ (fm)	$W_0$ (MeV)	$a_W$ (fm)	$\chi^2/N$	$\sigma_R$ (mb)	$J_V$ (MeV.fm <sup>3</sup> )	$J_W$ (MeV.fm <sup>3</sup> )
25	259.9	0.73	5.93	0.749	0.05	10.16	433.96	21.43
29	217.49	0.73	14.8	0.749	2.08	222.9	363.14	53.50
30	166.42	0.73	13.82	0.749	0.016	299.4	277.87	49.59
31	215.36	0.73	14.87	0.749	0.044	439.4	359.58	53.75
33	201.83	0.73	11.86	0.749	9.14	618.3	336.99	42.87
35	216.02	0.73	10.08	0.749	0.94	807.7	360.69	36.43
36	176.71	0.73	11.52	0.749	0.09	922.2	295.05	41.64
42	178.45	0.73	14.49	0.749	0.38	1500	297.96	52.37
43	164.51	0.834	26.0	0.534	0.54	1419	281.47	91.65
46	164.58	0.849	22.01	0.489	2.24	1528	251.59	77.25
48	201.48	0.73	19.09	0.749	0.36	1982	336.41	69.01
73.7	88.24	0.819	10.39	0.831	0.37	2726	150.42	37.97
88	75.46	0.811	9.49	0.939	2.8	3085	128.39	35.22
99	93.52	0.836	12.41	0.781	0.414	3098	160.09	45.05
156	41.27	0.93	11.53	0.852	0.95	3480	72.37	42.26
210	56.09	0.93	11.02	0.767	3.08	3428	98.36	39.93


 FIGURE 5. Comparison between  ${}^{208}\text{Pb}({}^6\text{Li}, {}^6\text{Li}) {}^{208}\text{Pb}$  elastic scattering angular distributions (solid circles) and SPP (solid curves) fits at  $E_{lab} = 25, 29, 30, 31,$  and  $33$  MeV. The data are displaced by  $0.5$  for the sake of clarity.

was taken as a factor times the real SPP. In other words, the calculations were performed using two free parameters, namely,  $N_{RSPP}$  (renormalization factor for the real part created based on SPP) and  $N_{ISPP}$  (renormalization factor for the imaginary part). The total potential in this case has the following form:

$$U(R) = V_C(R) - N_{RSPP} V^{DF}(R) - i N_{ISPP} V^{DF}(R). \quad (8)$$

As shown in Figs. 5-7, the agreement between the experimental  ${}^6\text{Li} + {}^{208}\text{Pb}$  angular distributions at energies


 FIGURE 6. Same as Fig. 5 but at  $E_{lab} = 35, 36, 42, 43, 46$  and  $48$  MeV. The data are displaced by  $0.2$  for the sake of clarity.

$25 - 210$  MeV and the calculations using real and imaginary SPP is fairly good. The optimal extracted potential parameters using this approach are listed in Table II, ( $J_V$ ), ( $J_W$ ), and ( $\sigma_R$ ) values are also presented.

The extracted  $N_{RSPP}$  value at the different considered energies is close to each other with an average value  $0.507 \pm 0.05$  except at energies  $25, 43,$  and  $46$  MeV. At  $E = 25$  MeV which is less than to  $E_C$ , the  $N_{RSPP}$  value is  $0.927$ . At energies  $43$  and  $46$  MeV, an anomaly is observed where the  $N_{RSPP}$  value is  $0.172,$  and  $0.104$  respectively. These results clearly show that, in order to reproduce the  ${}^6\text{Li} + {}^{208}\text{Pb}$  data, the strength of the real SPP should be reduced by about  $49\%$ .

TABLE II. Optimal potential parameters extracted from  ${}^6\text{Li} + {}^{208}\text{Pb}$  analysis using SPP for both real and imaginary parts. Real and imaginary volume integrals as well as reaction cross-sections are also listed.

$E$ (MeV)	$N_{RSPP}$	$N_{ISPP}$	$\chi^2/N$	$\sigma_R$ (mb)	$J_V$ (MeV.fm <sup>3</sup> )	$J_W$ (MeV.fm <sup>3</sup> )
25	0.927	0.187	0.05	8.556	377.41	76.13
29	0.522	0.736	2.07	226.5	211.62	298.38
30	0.42	0.694	0.017	303.0	170.09	281.05
31	0.518	0.752	0.044	441.8	209.55	304.21
33	0.49	0.615	8.91	619.5	197.80	248.26
35	0.524	0.521	0.97	802.2	211.08	209.87
36	0.452	0.578	0.08	912.1	181.88	232.58
42	0.45	0.697	0.26	1468	179.93	278.69
43	0.172	1.478	1.12	1779	68.70	590.34
46	0.104	2.245	3.23	2160	41.41	893.85
48	0.478	1.00	0.29	1973	189.41	396.25
73.7	0.541	0.58	0.63	2610	209.17	224.25
88	0.576	0.428	4.1	2715	219.37	163.01
99	0.515	0.574	0.21	2941	189.25	210.93
156	0.537	0.467	1.48	3115	190.48	165.65
210	0.568	0.599	15.4	3320	190.56	200.96

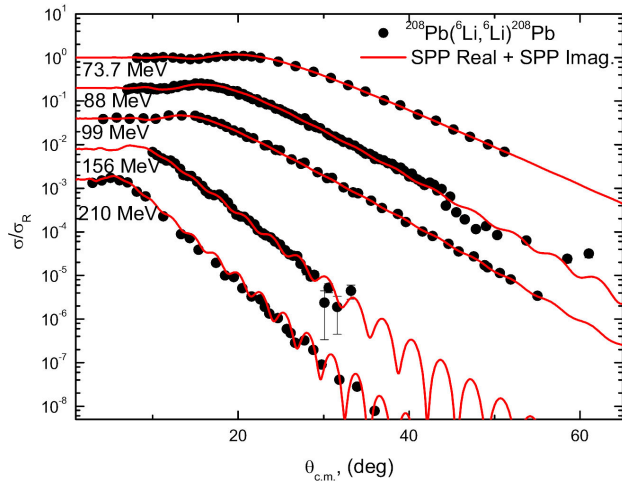


FIGURE 7. Same as Fig. 5 but at  $E_{lab} = 73.7, 88, 99, 156$  and  $210$  MeV. The data are displaced by 0.2 for the sake of clarity.

This reduction is essential to reproduce the experimental data for nuclear system induced by weakly bound nuclei such as  ${}^6\text{Li}$ ,  ${}^7\text{Li}$ , and  ${}^9\text{Be}$ .

The energy dependence on the obtained values for both the real  $J_V$  and imaginary  $J_W$  volume integrals from SPP calculations is illustrated in Fig. 8, which is based on the obtained values listed in Table II. The behavior deduced was fitted using the following equation:

$$J_{V,W}(E) = a + \frac{b}{E} + \frac{c}{E^2}. \quad (9)$$

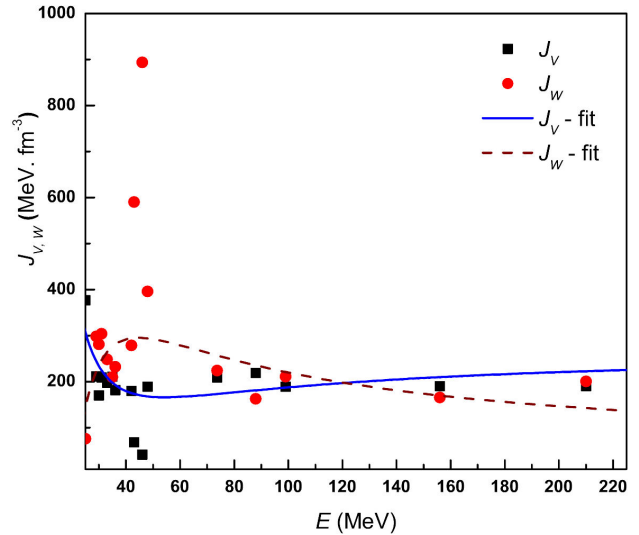


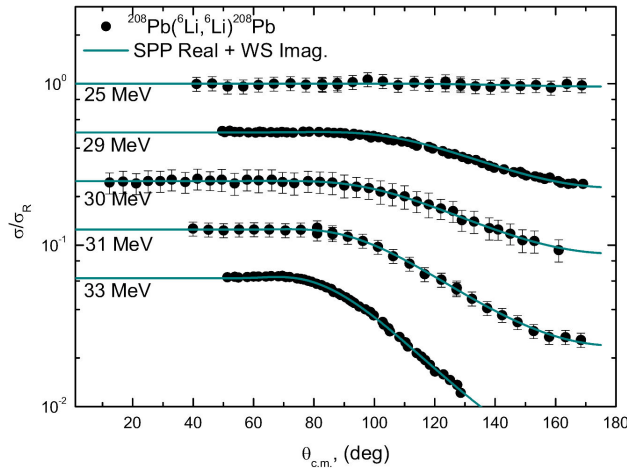
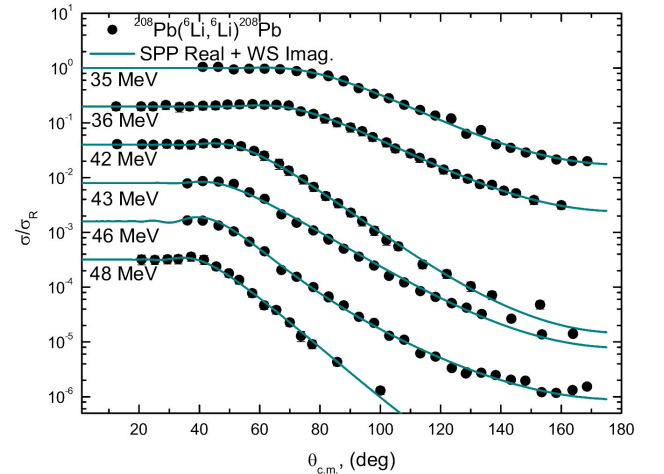
FIGURE 8. Energy dependence on volume integral for  ${}^6\text{Li} + {}^{208}\text{Pb}$  nuclear system.

With  $a = 269.09(49.1)$ ,  $b = -11186.6(21964.57)$ ,  $c = 303905.12(-489825.38)$  for real and imaginary volume integral respectively.

In the second approach, the real part of the potential was derived using SPP exactly as in the first approach in addition to an imaginary volume part in WS form to simulate the reduction in flux due to absorption, the radius parameter for the imaginary volume term was fixed at 1.7 fm similar to OM calculations. So, the calculations were performed using three parameters, namely,  $N_{RSPP}$  (renormalization factor for the real part created based on SPP), depth ( $W_0$ ) and diffuseness

TABLE III. Optimal potential parameters extracted from  ${}^6\text{Li} + {}^{208}\text{Pb}$  analysis using SPP for the real part +WS imaginary part. Real and imaginary volume integrals as well as reaction cross-sections are also listed.

$E$ (MeV)	$N_{RSPP}$	$W_0$ (MeV)	$a_W$ (fm)	$\chi^2/N$	$\sigma_R$ (mb)	$J_V$ (MeV.fm <sup>3</sup> )	$J_W$ (MeV.fm <sup>3</sup> )
25	0.993	3.844	0.747	0.05	6.842	404.28	13.89
29	0.748	13.19	0.703	11.6	184.9	303.25	47.39
30	0.362	13.84	0.749	0.017	299.5	146.60	50.02
31	0.523	14.85	0.732	0.05	422.5	211.57	53.55
33	0.489	13.59	0.714	8.4	607.6	197.39	48.90
35	0.428	9.84	0.788	0.87	833.9	172.41	35.75
36	0.482	12.26	0.696	0.07	878.4	193.95	44.01
42	0.398	13.7	0.745	0.43	1470	159.14	49.49
43	0.267	25.9	0.695	2.47	1636	106.65	92.97
46	0.799	22.17	0.488	2.21	1526	318.12	77.81
48	0.445	19.09	0.749	0.37	1978	176.33	69.01
73.7	0.433	10.71	0.799	0.41	2694	167.42	38.97
88	0.413	10.14	0.889	3.2	3048	157.29	37.37
99	0.395	12.32	0.798	0.43	3115	145.15	44.82
156	0.569	14.69	0.863	1.39	3681	201.83	53.93
210	0.324	14.96	0.893	8.8	3833	108.70	55.16


 FIGURE 9. Comparison between  ${}^{208}\text{Pb}({}^6\text{Li}, {}^6\text{Li}) {}^{208}\text{Pb}$  elastic scattering angular distributions (solid circles) and SPP for the real part +WS imaginary part (solid curves) fits at  $E_{lab} = 25, 29, 30, 31,$  and  $33$  MeV. The data are displaced by  $0.5$  for the sake of clarity.

 FIGURE 10. Same as Fig. 9 but at  $E_{lab} = 35, 36, 42, 43, 46$  and  $48$  MeV. The data are displaced by  $0.2$  for the sake of clarity.

( $a_W$ ) of the imaginary volume part. The total potential in this case has the following form:

$$U(R) = V_C(R) - N_{RSPP} V^{DF}(R) - iW(R). \quad (10)$$

As shown in Figs. 9-11, the agreement between the experimental  ${}^6\text{Li} + {}^{208}\text{Pb}$  angular distributions at energies  $25 - 210$  MeV and the calculations using real SPP and an imaginary WS potential is fairly good. The optimal extracted po-

tential parameters using this approach are listed in Table III, ( $J_V$ ), ( $J_W$ ), and ( $\sigma_R$ ) values are also presented. The average extracted  $N_{RSPP}$  value at the different considered energies is  $0.472 \pm 0.144$  except at energy  $25$  MeV. At  $E = 25$  MeV, the  $N_{RSPP}$  value is  $0.993$  which is close to the extracted value from the first approach. The observed anomaly at energies  $43$  and  $46$  MeV from the first approach is not exists in the results of the second approach. These results again emphasize that the strength of the real SPP should be reduced by about  $52\%$  in order to reproduce the  ${}^6\text{Li} + {}^{208}\text{Pb}$  data.

TABLE IV. Optimal potential parameters extracted from  ${}^6\text{Li} + {}^{208}\text{Pb}$  analysis using CFP for both real and imaginary parts. Real and imaginary volume integrals as well as reaction cross-sections are also listed.

$E$ (MeV)	$N_{RCF}$	$N_{ICF}$	$\chi^2/N$	$\sigma_R$ (mb)	$J_V$ (MeV.fm <sup>3</sup> )	$J_W$ (MeV.fm <sup>3</sup> )
25	0.532	0.1	0.05	11.00	216.59	40.71
29	0.64	0.414	2.96	230.6	259.46	167.84
30	0.494	0.439	0.015	316.6	200.06	177.79
31	0.489	0.529	0.06	470.5	197.82	214.01
33	0.442	0.477	19.7	654.0	178.43	192.56
35	0.386	0.517	0.82	881.4	155.49	208.26
36	0.307	0.581	0.15	1006	123.54	233.79
42	0.205	0.844	0.52	1659	81.97	337.47
43	0.1	0.779	10.4	1665	39.94	311.15
46	0.1	0.854	25.6	1905	39.82	340.02
48	0.147	1.11	0.52	2178	58.25	439.84
73.7	0.29	0.768	0.486	2833	112.13	296.94
88	0.367	0.672	3.4	2991	139.78	255.94
99	0.238	0.992	0.49	3345	87.46	364.53
156	0.296	0.789	0.93	3502	104.99	279.87
210	0.464	1.22	3.19	3921	155.67	409.31

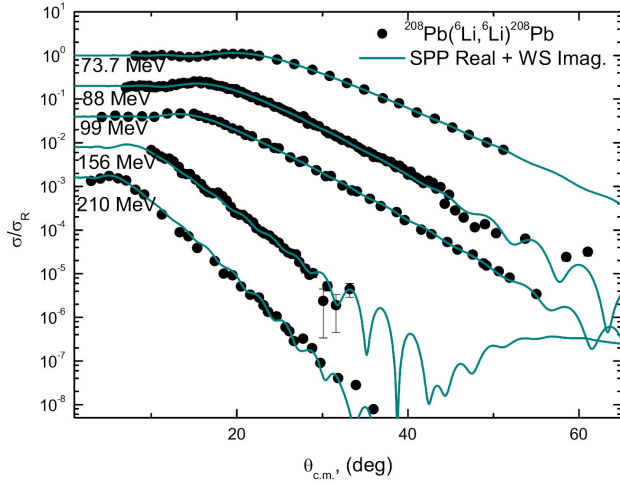


FIGURE 11. Same as Fig. 9 but at  $E_{lab} = 73.7, 88, 99, 156$  and  $210$  MeV. The data are displaced by  $0.2$  for the sake of clarity.

### 3.3. ${}^6\text{Li} + {}^{208}\text{Pb}$ data analysis using CF potential

Motivated by the well-known  $d + \alpha$  cluster structure for  ${}^6\text{Li}$ , we tried to reproduce the available experimental data for  ${}^6\text{Li} + {}^{208}\text{Pb}$  elastic scattering angular distributions using the fully microscopic cluster folding (CF) model. Within the framework of this model, the real and imaginary parts of potential were constructed based on CF potential (Eqs. 6 and 7). The total potential in this case has the following form:

$$U(R) = V_C(R) - N_{RCF}V^{CF}(R) - iN_{ICF}W^{CF}(R). \quad (11)$$

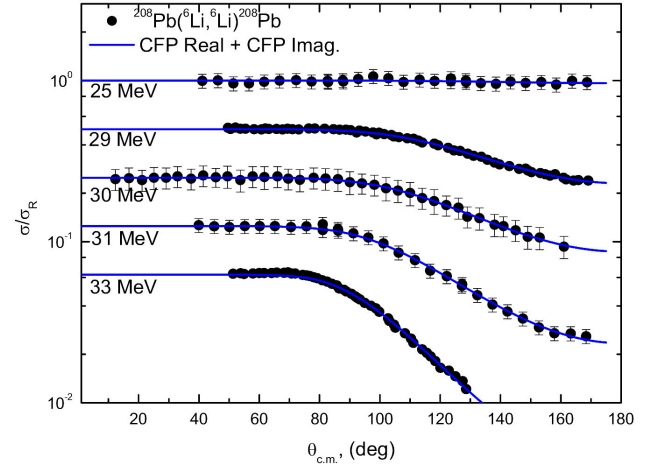
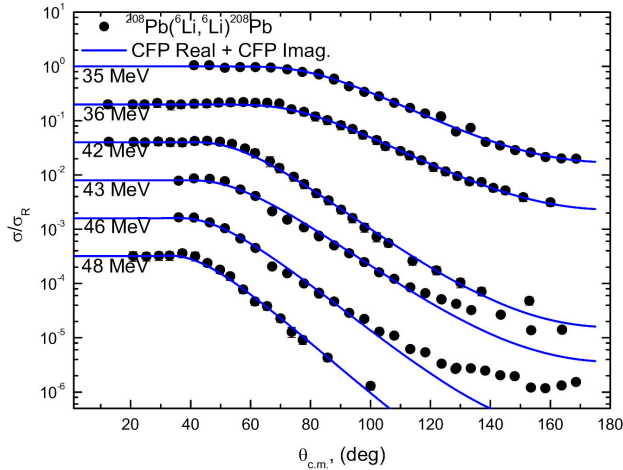


FIGURE 12. Comparison between  ${}^{208}\text{Pb}({}^6\text{Li}, {}^6\text{Li}){}^{208}\text{Pb}$  elastic scattering angular distributions (solid circles) and CFP (solid curves) fits at  $E_{lab} = 25, 29, 30, 31,$  and  $33$  MeV. The data are displaced by  $0.5$  for the sake of clarity.

The comparisons between the experimental  ${}^6\text{Li} + {}^{208}\text{Pb}$  elastic scattering angular distributions in the energy range  $25 - 210$  MeV [1–8] and the theoretical calculations within the framework of the CF model are shown in Figs. 12–14, with potential parameters listed in Table IV. The data are fitted using two parameters –  $N_{RCF}$  and  $N_{ICF}$  – renormalization factor for the real and imaginary CF potentials. To obtain good fitting with the experimental data, the strength of the real cluster folding potential should be reduced by  $\sim 62\%$ . In general, the observed reduction in the strength of the real part created based on either CF or DF is one of the signatures

TABLE V. Optimal potential parameters extracted from  ${}^6\text{Li} + {}^{208}\text{Pb}$  analysis using CFP for both real and imaginary parts with fixed  $N_{RCF} = 1.0$  plus DPP “surface potential with a repulsive part”.

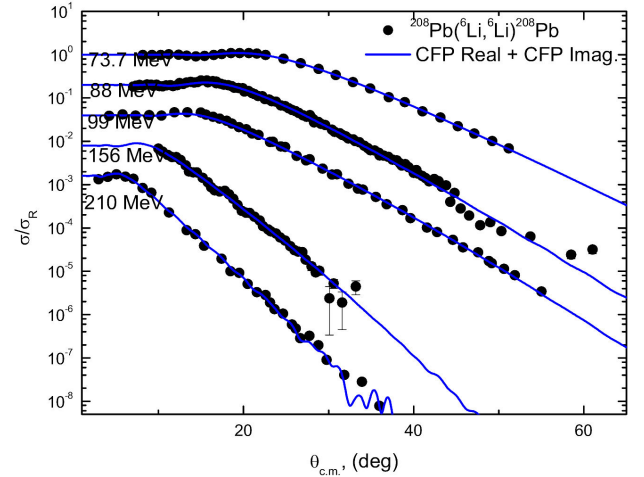
$E$ (MeV)	$N_{ICF}$	$V_{pol}$	$r_{pol}$	$a_{pol}$	$\chi^2/N$	$\sigma_R$ (mb)
25	0.1	-24.42	1.18	0.99	0.05	11.00
29	0.414	-20.88	1.18	0.98	3.08	231.0
30	0.439	-29.72	1.18	0.98	0.015	317.2
31	0.529	-30.1	1.18	0.98	0.06	471.1
33	0.477	-33.24	1.18	0.98	20.5	655.9
35	0.517	-36.67	1.18	0.98	0.82	884.1
36	0.581	-41.75	1.18	0.98	0.15	1008
42	0.844	-47.61	1.18	0.98	0.52	1661
43	0.779	-59.07	1.18	0.98	9.6	1652
46	0.854	-62.45	1.18	0.98	19.6	1882
48	1.11	-50.41	1.18	0.98	0.53	2180
73.7	0.768	-41.14	1.18	0.98	0.45	2844
88	0.672	-35.38	1.18	0.98	4.1	3009
99	0.992	-42.56	1.18	0.98	0.49	3358
156	0.789	-38.57	1.18	0.98	1.74	3522
210	1.22	-36.88	1.18	0.98	8.85	3920


 FIGURE 13. Same as Fig. 12 but at  $E_{lab} = 35, 36, 42, 43, 46$  and  $48$  MeV. The data are displaced by 0.2 for the sake of clarity.

for  ${}^6\text{Li}+X$  nuclear systems. The extracted average  $N_{RCF}$  is  $0.378 \pm 0.139$  from our CFM calculations. At energies 43 and 46 MeV, the data require more reduction in the strength of the real CF potential since the extracted  $N_{RCF} = 0.1$  at these two aforementioned energies. Such anomaly was also observed in the calculations using SPP first approach.

### 3.4. ${}^6\text{Li} + {}^{208}\text{Pb}$ data analysis using CFM plus a dynamical polarization potential

It is clearly shown from the current study and also previous studies concerning  ${}^6\text{Li} + {}^{208}\text{Pb}$  nuclear system that, the real


 FIGURE 14. Same as Fig. 12 but at  $E_{lab} = 73.7, 88, 99, 156$  and  $210$  MeV. The data are displaced by 0.2 for the sake of clarity.

real part of the potential constructed on microscopic procedures needs a renormalization by about 40-60 % in order to reproduce the experimental data. This reduction was assumed to be due to the break-up effect observed in the loosely bound  ${}^6\text{Li}$  nucleus. The analysis of  ${}^6\text{Li} + {}^{208}\text{Pb}$  elastic scattering data using real part of potential constructed on DF and CF procedures showed the same trend, in order to reproduce the data,  $N_{RCF}$  should be reduced by  $\sim 62$  %. This well-known reduction in the real DF and CF potentials' strength to reproduce the experimental data could be compensated by the introducing an additional dynamical polarization potential (DPP) of surface repulsive shape. This DPP simulates

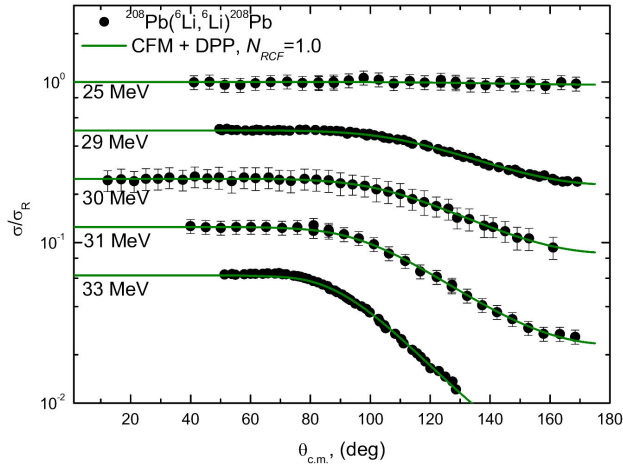


FIGURE 15. Comparison between  $^{208}\text{Pb}(^6\text{Li}, ^6\text{Li})^{208}\text{Pb}$  elastic scattering angular distributions (solid circles) and CFP fits with non-renormalized real cluster folding potential ( $N_{RCF} = 1$ ) plus a DPP term (solid curves) at  $E_{lab} = 25, 29, 30, 31,$  and  $33$  MeV. The data are displaced by 0.5 for the sake of clarity.

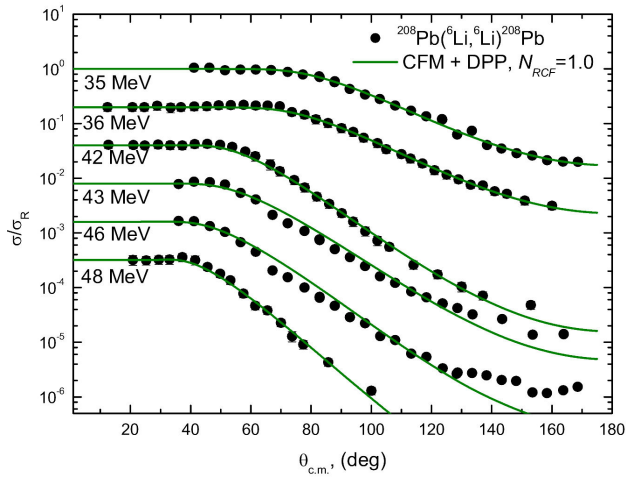


FIGURE 16. Same as Fig. 15 but at  $E_{lab} = 35, 36, 42, 43, 46$  and  $48$  MeV. The data are displaced by 0.2 for the sake of clarity.

the polarization effects caused by the break-up of the weakly bounded projectiles. The data are then reanalyzed using the following total potential:

$$U(R) = V_C(R) - N_{RCF} V^{CF}(R) - iN_{ICF} W^{CF}(R) + \Delta V_{pol}(R), \quad (12)$$

where the nuclear potential consists of three parts: a) real part derived from CF procedure without any renormalization ( $N_{RCF} = 1$ ), b) an imaginary CF potential with renormalization factor  $N_{ICF}$  fixed to the same values obtained from CFM analysis, and c) a dynamical polarization potential,  $\Delta V_{pol}(R)$  term which takes into account the dynamic contributions from all the allowed inelastic channels due to coupling. The DPP is taken as a surface potential with a repulsive real part and is characterized by three parameters

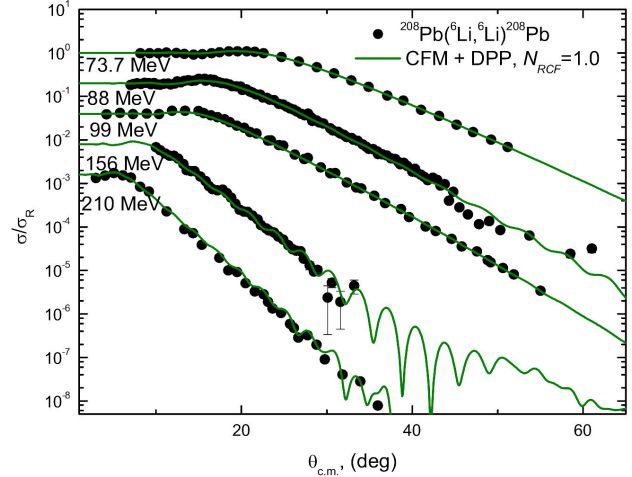


FIGURE 17. Same as Fig. 15 but at  $E_{lab} = 73.7, 88, 99, 156$  and  $210$  MeV. The data are displaced by 0.2 for the sake of clarity.

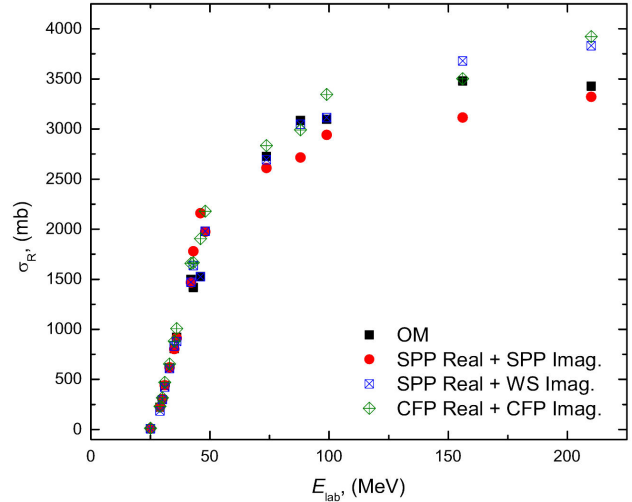


FIGURE 18. Energy dependence on reaction cross-section for  $^6\text{Li} + ^{208}\text{Pb}$  nuclear system.

( $V_{pol}$ ,  $r_{pol}$ ,  $a_{pol}$ ) and their corresponding values at the different concerned energies are listed in Table V. As shown in Figs. 15-17, the agreement between  $^6\text{Li} + ^{208}\text{Pb}$  experimental data and theoretical calculations constructed utilizing the non-renormalized real CFP plus DPP is fairly good except at  $E = 46$  MeV, where calculations showed some deviation especially at large angles.

The energy dependence on total reaction cross section ( $\sigma_R$ ) values extracted from OM, SPP Real + SPP Imag. (first approach), SPP Real + WS Imag. (second approach), and CFM calculations at the different concerned energies for  $^6\text{Li} + ^{208}\text{Pb}$  nuclear system is shown in Fig. 18. The extracted values for  $\sigma_R$  from the different implemented models are very close to each other especially at energies  $< 80$  and with a slight deviation at higher energies.

## 4. Summary

Experimental  ${}^6\text{Li}+{}^{208}\text{Pb}$  elastic scattering angular distributions at sixteen energy sets ranging from 25 MeV and up to 210 MeV are subjected to detailed analysis using different potentials constructed based on phenomenological, semi microscopic, and microscopic models. Firstly, 4-varying parameters OM calculations were successful in reproducing the concerned data. The nuclear potential has two parts: real and an imaginary volume term each has a WS shape of fixed radius parameter ( $r_V=1.3$  fm and  $r_W=1.7$  fm).

Then, the semi microscopic calculation based on a real potential part constructed using SPP2 REGINA code was performed in order to eliminate the ambiguities inherited in the phenomenological OM. Two approaches were used: in the first approach, the real part of the potential was derived using SPP and the imaginary part was taken as a factor times the real SPP. In the second approach, the real part of the potential was derived using SPP exactly as in the first approach in addition to an imaginary volume part has a WS form to

simulate the reduction in flux due to absorption. Calculations using the aforementioned two approaches showed the necessity to reduce the strength of the real part by  $\sim 49\%$  and  $52\%$  in order to reproduce the experimental data.

Finally, the fully microscopic CFM based on  $d + \alpha$  cluster structure for  ${}^6\text{Li}$  is tested. Reasonable fitting could be obtained if the strength of the real CF potential is reduced by  $\sim 62\%$ . The observed reduction in the real potential strength is mainly due to the  ${}^6\text{Li}$  break-up effect. CFM+DPP calculations are performed with non-renormalized real CF potential ( $N_{RCF}=1.0$ ) in addition to a repulsive real surface potential which takes into account the dynamic contributions from all the allowed inelastic channels due to coupling.

## Acknowledgement

A.A. Ibraheem extends his appreciation to the Deanship of Scientific Research at King Khalid University for funding this work through research groups program under grant number R.G.P.1/1/42.

- Zhang Chun-Lei *et al.*, *Unusual Threshold Anomaly in the  ${}^6\text{Li} + {}^{208}\text{Pb}$  System*; Chin. Phys. Lett. **23** (2006) 1146, <https://doi.org/10.1088/0256-307x/23/5/023>.
- N. Keeley *et al.*, *Optical model analyses of  ${}^{6,7}\text{Li} + {}^{208}\text{Pb}$  elastic scattering near the Coulomb barrier*, Nucl. Phys. A **571** (1994) 326 [https://doi.org/10.1016/0375-9474\(94\)90064-7](https://doi.org/10.1016/0375-9474(94)90064-7).
- H. Gemmeke, B. Deluigi, L. Lassen, and D. Scholz, *Coulomb and nuclear excitation in the sequential break-up of  ${}^6\text{Li}$* , Z. Physik A **286** (1978) 73.
- R. Huffman, A. Galonsky, R. Markham, and C. Williamson, *Elastic scattering of  ${}^6\text{Li}$  at 73.7 MeV*, Phys. Rev. C **22** (1980) 1522, <https://link.aps.org/doi/10.1103/PhysRevC.22.1522>.
- C. B. Fulmer *et al.*, *Elastic and inelastic scattering of 88 MeV  ${}^6\text{Li}$  ions*, Nucl. Phys. A **356** (1981) 235, [https://doi.org/10.1016/0375-9474\(81\)90125-1](https://doi.org/10.1016/0375-9474(81)90125-1),
- P. Schwandt *et al.*, *Optical potential for  ${}^6\text{Li}$  elastic scattering at 99 MeV*, Phys. Rev. C **24** (1981) 1522, <https://link.aps.org/doi/10.1103/PhysRevC.24.1522>
- J. Cook, H.J. Gils, H. Rebel, Z. Majka, and H. Klewe-Nebenius, *Optical model studies of  ${}^6\text{Li}$  elastic scattering at 156 MeV*, Nucl. Phys. A **388** (1982) 173 [https://doi.org/10.1016/0375-9474\(82\)90514-0](https://doi.org/10.1016/0375-9474(82)90514-0).
- A. Nadasen *et al.*, *Unique  ${}^6\text{Li}$  nucleosoptical potentials from elastic scattering of 210 MeV  ${}^6\text{Li}$  ions by  ${}^{28}\text{Si}$ ,  ${}^{40}\text{Ca}$ ,  ${}^{90}\text{Zr}$ , and  ${}^{208}\text{Pb}$* , Phys. Rev. C **39** (1989) 536. <https://link.aps.org/doi/10.1103/PhysRevC.39.536>.
- K. Schwarz *et al.*, *Reaction mechanism of  ${}^6\text{Li}$  scattering at 600 MeV*, Eur. Phys. J. A **7** (2000) 367, <https://doi.org/10.1007/PL00013619>.
- C. Signorini *et al.*, *Exclusive breakup of  ${}^6\text{Li}$  by  ${}^{208}\text{Pb}$  at Coulomb barrier energies*, Phys. Rev. C **67** (2003) 044607, <https://link.aps.org/doi/10.1103/PhysRevC.67.044607>.
- Yongli Xu *et al.*,  *${}^6\text{Li}$  global phenomenological optical model potential*, Phys. Rev. C **98** (2018) 024619, <https://link.aps.org/doi/10.1103/PhysRevC.98.024619>.
- S. Hossain, M. N. A. Abdullah, Md. Zulfiker Rahman, A. K. Basak and F. B. Malik, *Non-monotonic potentials for  ${}^6\text{Li}$  elastic scattering at 88 MeV*, Phys. Scr. **87** (2013) 015201, <https://doi.org/10.1088/0031-8949/87/01/015201>.
- Pang Dan-Yang, *Effects of relativistic kinematics in heavy ion elastic scattering*, Chinese Physics C **38** (2014) 024104, <https://doi.org/10.1088/1674-1137/38/2/024104>.
- M. El-Azab Farid and M.A. Hassanain, *Folding model analysis of  ${}^{6,7}\text{Li}$  elastic scattering at 12.5-53 MeV/u*, Nucl. Phys. A **697** (2002) 183 [https://doi.org/10.1016/S0375-9474\(01\)01244-1](https://doi.org/10.1016/S0375-9474(01)01244-1).
- J. Cook, *The energy dependence of  ${}^6\text{Li}$  optical potentials*, Nucl. Phys. A **375** (1982) 238, [https://doi.org/10.1016/0375-9474\(82\)90411-0](https://doi.org/10.1016/0375-9474(82)90411-0).
- C. J. Lin *et al.*, *Effects of breakup of weakly bound projectile and neutron transfer on fusion reactions around Coulomb barrier*, Nucl. Phys. A **787** (2007) 281, <https://doi.org/10.1016/j.nuclphysa.2006.12.044>.
- Shin Watanabe *et al.*, *Four- and three-body channel coupling effects on  ${}^6\text{Li}$  elastic scattering with CDCC*, EPJ Web of Conferences **113** 06007 (2016) <https://doi.org/10.1051/epjconf/201611306007>.
- Jin Lei and Antonio M. Moro, *Comprehensive analysis of large  $\alpha$  yields observed in  ${}^6\text{Li}$ -induced reactions*, Phys. Rev. C

- 95 (2017) 044605, <https://link.aps.org/doi/10.1103/PhysRevC.95.044605>.
19. D. R. Otomar, P. R. S. Gomes, J. Lubian, L. F. Canto, and M. S. Hussein, *Nuclear and Coulomb breakup of the weakly bound  ${}^6\text{Li}$  nucleus with targets in the range from  $A = 59$  to 208*, Phys. Rev. C **87** (2013) 014615, <https://link.aps.org/doi/10.1103/PhysRevC.87.014615>.
  20. N. Keeley, K. W. Kemper, and K. Rusek, *Dynamic polarization potentials and dipole polarizabilities of  ${}^{11}\text{Li}$ ,  ${}^6\text{He}$  and  ${}^6\text{Li}$  compared*, Phys. Rev. C **88** (2013) 017602, <https://link.aps.org/doi/10.1103/PhysRevC.88.017602>.
  21. Y. Kucuk, I. Boztosun, and N. Keeley, *Onset of nuclear structure effects in near-barrier elastic scattering of weakly bound nuclei:  ${}^6\text{He}$  and  ${}^6\text{Li}$  compared*, Phys. Rev. C **79** (2009) 067601. <https://link.aps.org/doi/10.1103/PhysRevC.79.067601>.
  22. S. K. Patra, R. N. Panda, P. Arumugam, and Raj K. Gupta, *Nuclear reaction cross sections of exotic nuclei in the Glauber model for relativistic mean field densities*, Phys. Rev. C **80** (2009) 064602, <https://link.aps.org/doi/10.1103/PhysRevC.80.064602>.
  23. K. Rusek, N. Alamanos, N. Keeley, V. Lapoux, and A. Pakou, *Breakup and fusion of  ${}^6\text{Li}$  and  ${}^6\text{He}$  with  ${}^{208}\text{Pb}$* , Phys. Rev. C **70** (2004) 014603 <https://link.aps.org/doi/10.1103/PhysRevC.70.014603>.
  24. C. Samanta, Y. Sakuragi, M. Ito and M. Fujiwara, *Energy dependence of the  ${}^6\text{Li}$  - nucleus interactions at intermediate energies*, J. Phys. G: Nucl. Part. Phys. **23** (1997) 1697 <https://doi.org/10.1088/0954-3899/23/11/017>.
  25. N. Keeley and K. Rusek, *The role of breakup in near-barrier  ${}^6\text{Li}+{}^{208}\text{Pb}$  scattering*, Phys. Lett. B **375** (1996) 9 [https://doi.org/10.1016/0370-2693\(96\)00263-8](https://doi.org/10.1016/0370-2693(96)00263-8).
  26. A. Pakou *et al.*, *Important influence of single neutron stripping coupling on near-barrier  ${}^8\text{Li} + {}^{90}\text{Zr}$  quasi-elastic scattering*, EPJA **51** (2015) 90 <https://doi.org/10.1140/epja/i2015-15090-3>.
  27. M. Mazzocco *et al.*, *Direct and compound-nucleus reaction mechanisms in the  ${}^7\text{Be} + {}^{58}\text{Ni}$  system at near-barrier energies*, Phys. Rev. C **92** (2015) 024615, <https://link.aps.org/doi/10.1103/PhysRevC.92.024615>.
  28. I. Lombardo *et al.*, *Study of Nuclear Structure of  ${}^{13}\text{C}$  and  ${}^{20}\text{Ne}$  by Low Energy Nuclear Reactions*, Journal of Physics: Conference Series **569** (2014) 012068 <https://doi.org/10.1088/1742-6596/569/1/012068>.
  29. Sh. Hamada and Awad A. Ibraheem, *Peculiarities of  ${}^6\text{Li}+{}^{12}\text{C}$  elastic scattering*, Int. J. Mod. Phys. E **28** (2019) 1950108, <https://doi.org/10.1142/S0218301319501088>.
  30. Sh. Hamada *et al.*, *Analysis of  ${}^6\text{Li}+{}^{16}\text{O}$  elastic scattering using different potentials*, Rev. Mex. Fis. **66** (2020) 322, <https://doi.org/10.31349/RevMexFis.66.322>.
  31. Sh. Hamada and Awad A. Ibraheem, *Cluster folding optical potential analysis for  ${}^6\text{Li}+{}^{28}\text{Si}$  elastic scattering*, Rev. Mex. Fis. **67** (2021) 276, <https://doi.org/10.31349/RevMexFis.67.276>.
  32. Sh. Hamada, Norah A. M. Alsaif and Awad A. Ibraheem, *Detailed analysis for  ${}^6\text{Li}+{}^{40}\text{Ca}$  elastic scattering using different potentials*, Phys. Scr. **96** (2021) 055306 <https://doi.org/10.1088/1402-4896/abeba6>.
  33. I. J. Thompson, *Coupled reaction channels calculations in nuclear physics*, Comput. Phys. Rep. **7** (1988) 167 [https://doi.org/10.1016/0167-7977\(88\)90005-6](https://doi.org/10.1016/0167-7977(88)90005-6).
  34. L. C. Chamon *et al.*, *Nonlocal Description of the Nucleus-Nucleus Interaction*, Phys. Rev. Lett. **79** (1997) 5218. <https://link.aps.org/doi/10.1103/PhysRevLett.79.5218>.
  35. L. C. Chamon, D. Pereira, M. S. Hussein, *Parameterfree account of quasielastic scattering of stable and radioactive nuclei*, Phys. Rev. C **58** (1998) 576, <https://link.aps.org/doi/10.1103/PhysRevC.58.576>.
  36. L.C. Chamon, *The Sao Paulo Potential* Nucl. Phys. A **787** (2007) 198. <https://doi.org/10.1016/j.nuclphysa.2006.12.032>.
  37. L. C. Chamon, B. V. Carlson and L. R. Gasques, *Sao Paulo potential version 2 (SPP2) and Brazilian nuclear potential (BNP)*, Comp. Phys. Comm. **267** (2021) 108061 <https://doi.org/10.1016/j.cpc.2021.108061>.
  38. B. V. Carlson and D. Hirata, *Dirac-Hartree-Bogoliubov approximation for finite nuclei*, Phys. Rev. C **62** (2000) 054310 <https://link.aps.org/doi/10.1103/PhysRevC.62.054310>.
  39. G. Duhamel *et al.*, *Diffusion élastique et inélastique de deutons de 80 MeV*, Nucl. Phys. A **174** (1971) 485 [https://doi.org/10.1016/0375-9474\(71\)90398-8](https://doi.org/10.1016/0375-9474(71)90398-8).
  40. D. A. Goldberg *et al.*, *Scattering of 139 MeV Alpha Particles by  ${}^{58}\text{Ni}$  and  ${}^{208}\text{Pb}$* , Phys. Rev. C **7** (1973) 1938 <https://link.aps.org/doi/10.1103/PhysRevC.7.1938>.